Monitoring Displacement Distribution within the Rock Mass during a Plate Load Test

A.B. Huang, J.J. Liao, I.W. Pan, and C.P. Lin
Department of Civil Engineering, National Chiao Tung University, Hsin Chu, TAIWAN

ABSTRACT: A fiber optic sensor system has been developed specifically for monitoring displacements within geomaterials. Optic fiber Bragg gratings were fixed to the sides of a slender piece of plastic rod as a means for displacement measurements. An attempt was made to monitor the local displacements within an artificial soft rock sample in a laboratory model plate load test. Two 8 mm diameter fiber optic sensored Delrin rods were inserted into the rock mass at various depths below the model foundation. The amount and distribution of the displacements caused by the plate load were measured through the flexural strains occurred in the fiber optic sensors. Initial results have indicated that the technique was capable of detecting relative displacements at least for the case of a model plate load test. Reasonable relationship between moduli and strains could be derived from these displacement measurements and estimated average stresses based on Boussinesq theory. This paper describes the laboratory set up of the sensor system; present the results of the plate load test and discusses the implications in the use of fiber optic sensors for field local displacement measurements.

1 INTRODUCTION

The value and necessity of local displacement measurements for laboratory tests have been well accepted. Field local displacement measurements underneath a loaded foundation have been an important part of the development in recognizing the meaning of small strain stiffness of geomaterials (Burland, 1989). An important aspect of local displacement, both in case of field and laboratory measurements, is that it is free from bedding effects of boundary loads. In his closing remarks, Burland (1995) posted a challenge to develop a simple and ingenious way of carrying out such measurements.

The authors developed a technique that combines fiber optic sensors and the concept of strain pipes to monitor displacements within a geomaterial. A series of optic Fiber Bragg Gratings (FBG) were fixed to a flexible rod to sense the flexural strains experienced by the FBG as the rod was deformed by bending. Integrating strains with respect to distance would yield displacement in the transverse direction of the rod. If the FBG sensored rod is strategically embedded in the geomaterial so that material movement could cause bending of the rod, then it would serve the purpose of displacement measurements. The sensitivity and range of displacement that can be monitored by the sensor rod can be adjusted by varying the diameter and length of the rod. The same system can be used for laboratory model test or field monitoring.

This paper describes the details of an FBG displacement sensing system and presents a case where it is used to monitor distribution of ground displacement within an artificial soft rock during a model plate load test.

2 THE DISPLACEMENT SENSING SYSTEM

2.1 *Optic Fiber Bragg Grating Strain Sensors*

Optic fiber is typically made of silica or glass with a diameter on the order of 125 μm. Usually the optic fiber is protected by a layer of coating, making the total diameter of the fiber close to 250 μm. The optic signals are immune to electro-magnetic noise. Thus, using optic fiber as a sensor can have many potential advantages. The optic Fiber Bragg grating (FBG) is one of many types of currently available fiber optic sensors. Hill et al. (1978) suggested that gratings can be generated by sustained exposure of an optic fiber core to laser radiation under a controlled pattern of interference. Following this concept, various techniques of producing in-fiber Bragg grating (FBG) sensors have been developed over the last decade. The length of FBGs is normally within

the range of 10 to 30 mm. A periodic variation of fiber core refractive index is formed by exposing that 10 to 30 mm segment of single mode optic fiber to a spatial pattern of ultraviolet light. When the FBG is illuminated by a wideband light source, a fraction of the light is reflected back upon interference by the FBG. The wavelength of the reflected light, or the Bragg wavelength, λ_B is related to the period of the index modulation, Λ and effective fiber core index of refractive, n as

$$\lambda_B = n\Lambda \tag{1}$$

Longitudinal strains within the Bragg grating, ε_B induced by variations in temperature or stress can cause a change in Λ and thus a shifting of λ_B, with the following approximate relationships (Rao, 1998):

$$\Delta\lambda_B = 0.74\lambda_B\varepsilon_B \tag{2}$$

and

$$\Delta\lambda_B = 8.9\times10^{-6}\lambda_B\Delta^oC \tag{3}$$

where Δ^oC is the change of temperature in degree Celsius. The constants in Equations (2) and (3) can vary, depending on the photoelastic properties of the optic fiber. For the FBG reported herein, λ_B ranged from 1525 to 1575 nm (10^{-9}m). The returned signal from every FBG carries a unique range or domain of wavelength $\lambda_B + \Delta\lambda_B$, making it possible to have multiple FBG elements on the same fiber. The multiplexing among various sensors on a single fiber can be accomplished by wavelength division addressing as conceptually described in Figure 1. Most of the silica optic fiber breaks at a strain of approximately 0.01 which corresponds to a $\Delta\lambda_B$ of approximately 10 nm. Thus, a separation of λ_B in 2 to 3 nm between FBGs would suffice in most cases. There is a limited bandwidth of the light source and as the light passes an FBG there is a loss of its intensity, the number of FBG sensors that can be placed on a fiber is not more than 20 with the currently available FBG interrogation systems.

2.2 *The Pipe Strain Gage*

Takada (1965) has reported the idea of a pipe strain gage to measure ground displacement. A series of strain gages are attached to the outside of a plastic pipe at constant intervals. This instrumented pipe is then grouted in the ground. The strain gages measure the flexural strains, ε experienced by the pipe as it is forced to deform with the ground. According to the mechanics of materials,

$$M = \frac{\varepsilon}{r}EI \tag{4}$$

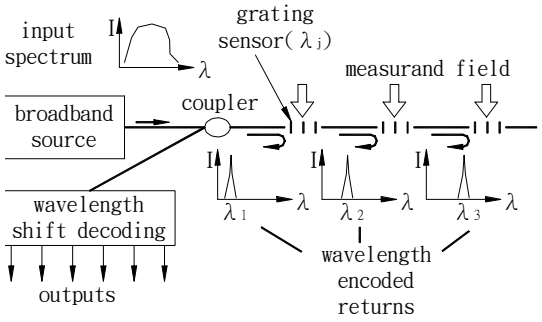

Figure 1. A conceptual description of FBG sensors (after Kersey, 1992).

and

$$\frac{d^2y}{dx^2} = \frac{M}{EI} \tag{5}$$

where

M= bending moment experienced by the pipe;
r = outside radius of the pipe;
E = Young's modulus of the pipe material;
I = moment of inertia of the pipe;
x = depth; and
y = lateral displacement

Thus,

$$\frac{d^2y}{dx^2} = \frac{\varepsilon}{r} \tag{6}$$

The pipe inclination, dy/dx is related to ε as

$$\frac{dy}{dx} = \frac{1}{r}\int\varepsilon dx + e \tag{7}$$

and

$$y = \frac{1}{r}\int\left(\int\varepsilon dx\right)dx + eX + f \tag{8}$$

where e and f are integration constants and X represents the full length of the pipe. Equation (8) presents a mathematical relationship between ε and y. In order to carry out the integrations, it is necessary to assume a linear interpolation between the discrete strain measurements or use cubic Spline functions to fit the data points. Although theoretically sound, it is rather difficult to implement pipe strain gages in the field. Every strain gage demands a separate cable for power supply and signal transmission. Unless the pipe and the borehole are unusually large, the number of strain gages and thus the signal cables that can be placed underground is rather limited. The signals generated from the strain gages are subject to electro-magnetic noise possibilities of short circuit. It is likely due to these serious drawbacks, the pipe strain gages have not been widely accepted

as a primary instrument to monitor ground movements.

2.3 *The FBG sensor rod*

With its small size and the capability of multiplexing, the FBG is ideal for instruments where multiple sensors are required. An FBG sensored pipe strain gage can be equipped with many strain measurement points, without the hazards of electronic/mechanical parts or bulky cables. A fiber Bragg grating Swept Laser Interrogator (Micron Optics, Inc., Atlanta, Georgia), SLI was used to take FBG strain readings. A minimum change in λ_B of approximately 1 pm (pico meter or 10^{-12}m) that corresponds to <1 $\mu\varepsilon$ can be resolved with the SLI. The interrogating system has the capacity to simultaneously scan four optic fibers, each with a maximum of 64 FBG's at a rate of 104 Hz. The FBG readings from SLI are transmitted to a notebook computer in digital form through a PCMCIA interface card. For the case reported herein, a 320mm long and 8mm diameter Delrin rod with a total of 7 FBG's distributed on two opposite sides of the Delrin rod were used. Figure 2 shows a photograph of a FBG sensor rod.

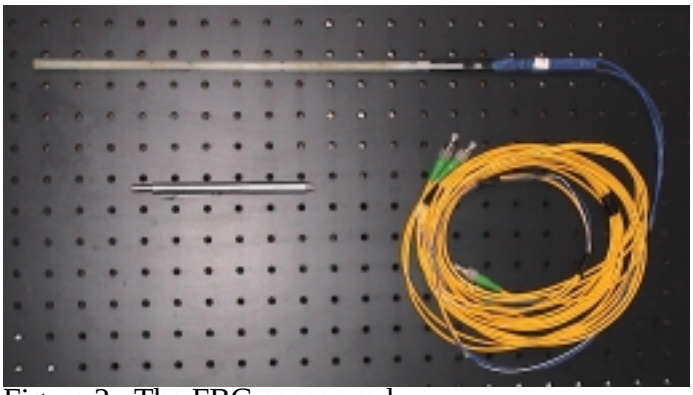

Figure 2. The FBG sensor rod.

3 THE MODEL PLATE LOAD TEST

3.1 *Preparation of the artificial soft rock sample*

The model plate load test was performed on an artificially prepared soft rock. A young weakly cemented sandstone from Hsin Chu area was pulverized and converted into a silty fine sand. The specific gravity of the sand was 2.61. Figure 3 shows the grain size distribution of the sand. Particles passing No. 30 sieve were used to make the artificial sandstone. To assure repeatability, the minus No. 30 sand was then washed through a No. 200 sieve. The artificial rock was made of a blend in 1:1 ratio by dry weight of particles retained and passed No.200 sieve. The sand/silt was then mixed into a slurry with 26% of water content. The soft rock was created by consolidating the slurry in a 600 mm long, 300 mm wide and 650 mm deep test box with rigid lateral boundaries, under a vertical load where drainage was allowed on top and bottom of the sample. Figure 4 shows the arrangement of the plate load test load frame and the sample box. For the test reported herein, the sample was consolidated under 981 kN of vertical force for 5 days. The side walls of the consolidation mold were then removed and the sample was air dried for a week. The consolidated sample had a height of approximately 450 mm. A 50 mm wide, 300 mm long and 100 mm thick model plate, made of solid steel was used to simulate a rigid strip foundation on the surface of the rock sample.

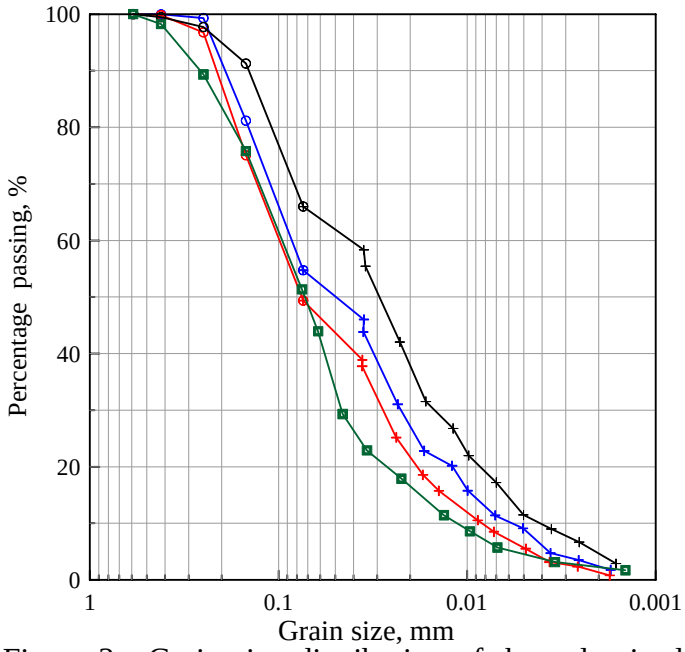

Figure 3. Grain size distribution of the pulverized sandstone.

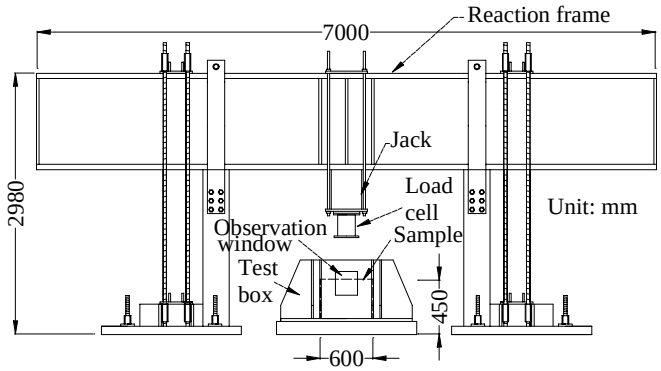

Figure 4. The loading system.

Upon drying of the rock sample, a grid pattern of 10x10 mm was marked on the front (600x450 mm side) face of the sample and a different set of side walls were assembled around the sample. These side walls were designed specifically for the plate load test. The steel plate within an area of 300x300 mm on the front face of the sample box was replaced with a 15mm thick plastic sheet so that movement of the rock mass immediately under the model foundation can be seen from the outside. A 10 mm wide

and 150 mm long slot was located in the middle of the sidewall (300x450 mm side) to allow insertion of the FBG sensor rods.

3.2 *Installation of the FBG sensor rods and model plate load test*

Because of the high cost, it was necessary that the FBG sensor rods could be retrieved after serving their purpose and reused. Upon reassembling the sample in the test box, two 300mm deep, 12mm diameter holes were bored horizontally from the open slot on the side wall. The boreholes were filled with freshly mixed plaster of Paris. The FBG sensor rods were inserted into the boreholes before the plaster hardened, thus filling the annular space between the FBG sensor rod and the borehole wall. The FBG sensor rod was coated with a thin film of engine oil and then covered with a sheet of plastic wrap. The above arrangements assured intimate contact between the FBG sensor rod and the rock mass, and also allowed the rods be retrieved without breaking the rock sample. The two FBG sensor rods were located at 30 and 60 mm below the model plate, respectively as schematically shown in Figure 5. These two rods were designated as Rod a and Rod b, respectively as shown in Figure 5.

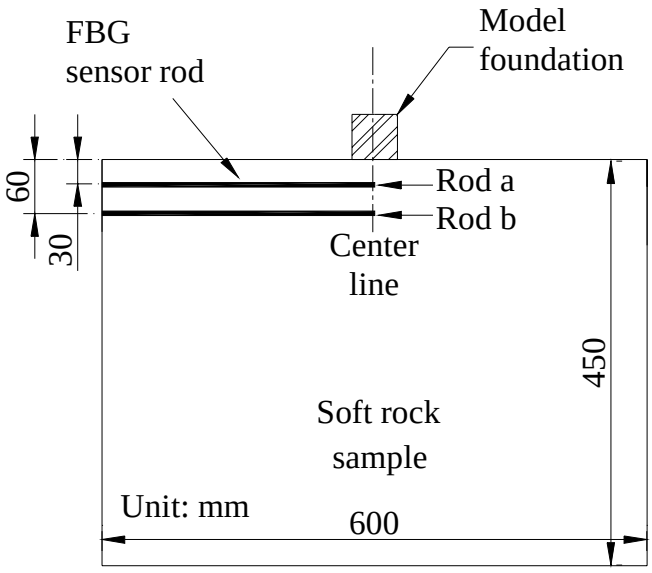

Figure 5. Locations of the FBG sensor rods.

Figure 6 shows the laboratory setup during the plate load test. A digital video camera pointing at the observation widow (see Fig. 4) was used to record the movement pattern of the rock mass throughout the load test. The plate load test was stress controlled and performed in close conformance with the ASTM standard D1194. The plate load test was interrupted when the bearing pressure reached 4.97 MPa. At this stage, the FBG sensor rods had not experienced sufficient bending to cause permanent damage. Upon releasing the bearing pressure, the FBG sensor rods were retrieved and the holes filled with plaster. The plate load test was then resumed and continued until failure. The settlement of the model foundation was monitored with an LVDT throughout the test.

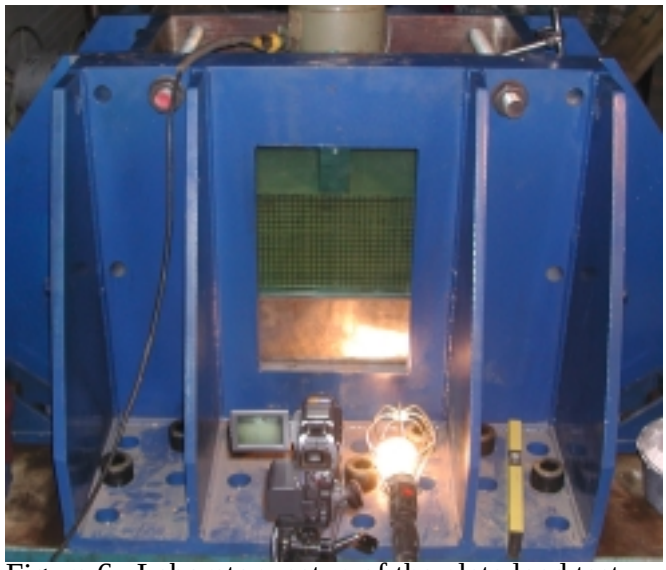

Figure 6. Laboratory setup of the plate load test.

4 RESULTS AND ANALYSIS

4.1 *Displacement distribution*

Figure 7 shows the load settlement curve of the plate load test according to the load cell and LVDT readings. The wave length, λ_B reflected from all the FBG's embedded in the sample along with the sensor rods were converted to flexural strain, ε_B according to Equation 2. A set of reference ε_B values was recorded just prior to the load test. The displacement of the sensor rod in the vertical direction (perpendicular to the direction of the sensor rod) was then computed using Equation 8, based on the differences of ε_B as compared to the initial values recorded prior to the load test. The integration assumed no bending or rotation of the sensor rod at the stem, located at the outside of the rock sample. Figure 8 depicts the profiles of displacements inferred from the FBG readings at various stages of bearing pressures. The FBG had a length of 28mm. The distance values shown in Figure 8 represent the center position of the individual FBG's. Unstable readings were recorded in FBG's of Rod a, when the bearing pressure exceeded 1.57 MPa. Their results are thus not displayed in Figure 8. The displacements generally increased with bearing pressure. In general, the displacement was more significant in Rod a than Rod b, as it should be, since Rod a was closer the foundation. The load test was interrupted when the bearing pressure reached 4.97 MPa. At that stage the foundation at the ground surface settled ap-

proximately 2.5mm. After recording all the instrumentation readings, the bearing pressure was reduced to zero and the FBG sensor rods removed. The holes were backfilled with plaster.

Cracks started appearing during the stage of bearing pressure release. The cracks became more distinctive as the load test was resumed and the bearing pressure increased beyond 4.97 MPa. The load test was terminated when the bearing pressure reached 12 MPa. Figure 9 shows a photograph taken at the observation window towards the end of load test, revealing the failure pattern of the rock. Relative displacement and thus bending of the FBG sensor rod across the crack surface was likely to be very significant. This could be the reason for damaging unstable readings in Rod a at an early stage of the load test.

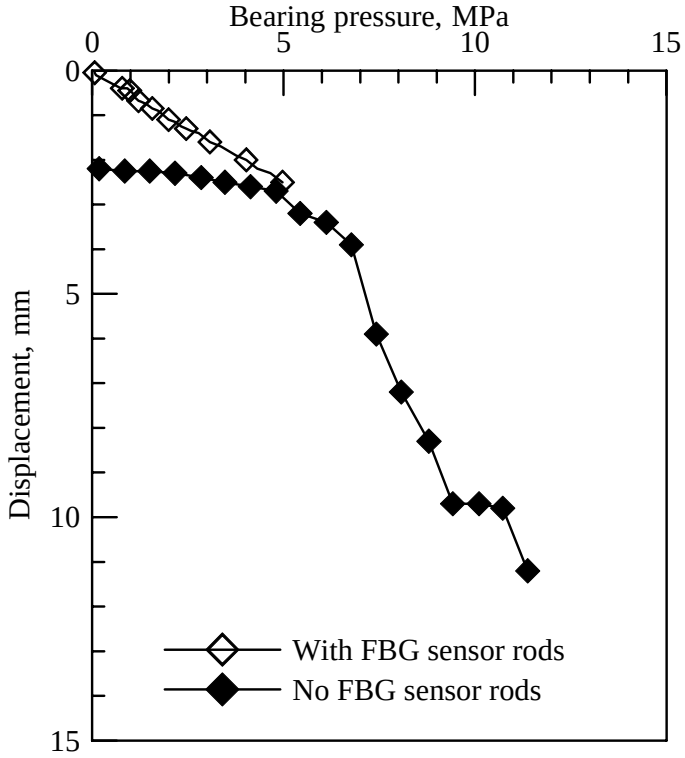

Figure 7. The load settlement curve.

4.2 *Analysis of the test data*

Following the plate load test, NX sized rock cores were taken in the horizontal and vertical directions from the artificial rock sample. Care was taken to recover cores in areas where cracks were not present. These cores were used to measure water contents, densities, unconfined compressive strengths and shear wave velocities using bender elements. The rock cores had an average water content of 2.66%, and a dry unit weight of 18.93 kN/m^3. The maximum Young's modulus, E_o according to the shear wave velocity measurements and an assumed Poisson's ratio of 0.3, was approximately 2800 MPa. The unconfined compressive strengths, q_u for rock cores taken in the horizontal direction varied from 2.6 to 3.1 MPa. The value of q_u for the rock core taken in the vertical direction was 4.2 MPa.

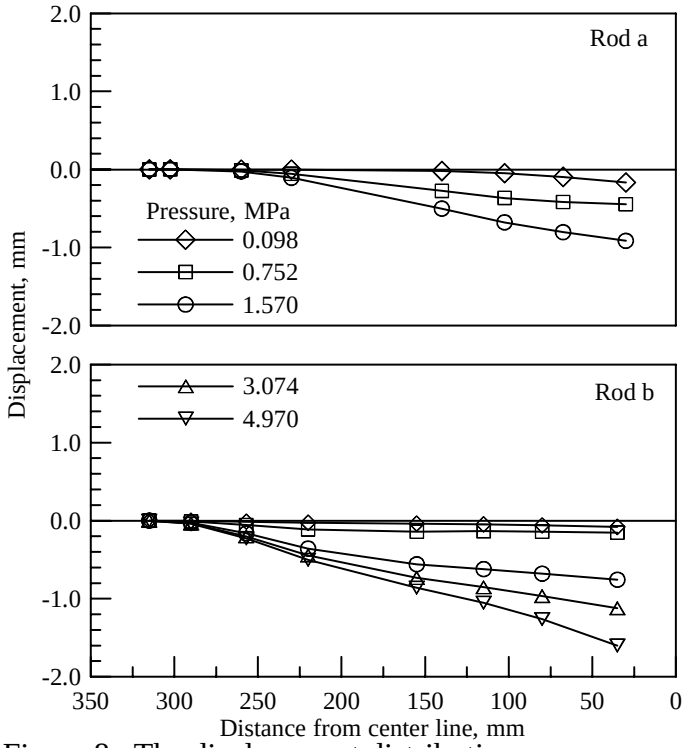

Figure 8. The displacement distribution.

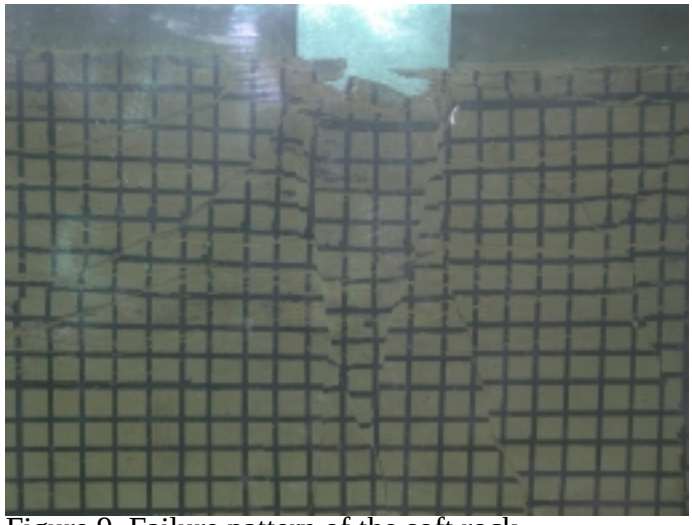
Figure 9. Failure pattern of the soft rock.

Estimations of the average stresses and strains under the model foundation were made using the Boussinesq theory and the local displacement measurements by the FBG sensor rods. Computations of stresses and strains were limited to points along a vertical line directly under the left edge of the model foundation, at 25 mm from the center line (see Figure 5). The average strains were computed based on relative displacements and distances among Rod a, Rod b and the bottom of the model foundation. The center of the first FBG was at 30 to 35 mm from the center line as depicted in Figure 8. The FBG sensor rod readings were linearly extrapolated to estimate the displacement at 25 mm from the center line at the depth where the

the depth where the sensor rod was located. The corresponding average stress was calculated at the mid-point between the two target locations (e.g. Rod a and bottom of the foundation, etc.). With these stress and strain values, a set of Young's moduli and the corresponding strains were obtained. A plot of these Young's moduli versus the average strains, along with the maximum Young's modulus, E_o from the seismic wave velocity measurements on the rock cores are shown in Figure 10. The results showed a rather consistent and reasonable degrading relationship between moduli and strains. The Young's moduli estimated according to the foundation bearing pressure-settlement relationship shown in Figure 7 using the elastic solution and an assumed Poisson's ratio of 0.3, were on the order of 180 to 190 MPa, for bearing pressures less than 4.97 MPa. These moduli should correspond to an average strain between 0.1 and 0.5 % according to Figure 10. These values are well within the range of strains expected for a soft rock under pre-failure loading conditions.

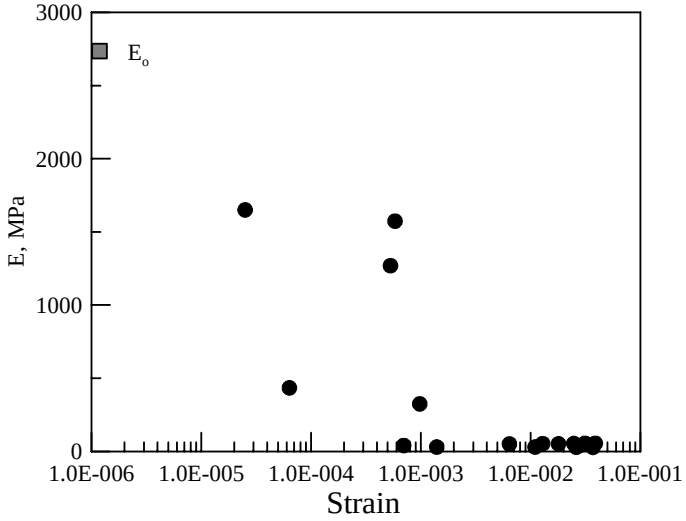

Figure 10. Modulus degradation according to the displacement readings.

5 CONCLUSIONS

An attempt has been made to monitor local displacements within the geomaterial using fiber optic sensors. Initial results have indicated that the technique is capable of detecting relative displacements at least for the case of a model plate load test. Reasonable relationship between moduli and strains could be derived from these displacement measurements and estimated average stresses based on the Boussinesq theory. The sensitivity and range of displacement measurements can be adjusted by varying the diameter and length of the rod that the fiber optic sensors are mounted on. Thus, the technique should be equally applicable for field applications where the dimensions of loading dimensions of loading elements and displacements are likely to be significantly larger.

6 ACKNOWLEDGEMENTS

Funding for this research was provided by the Ministry of Education, Center of Excellence research program on "Photonic Science and Technology for the Tera Era" and National Science Council of ROC under contracts No. 89-2218-E-009-102, 89-2218-E-009-105, and 90-2611-E-009-007.

7 REFERENCES

Burland, J.B., 1989. Small is Beautiful, Ninth Laurits Bjerrum Memorial Lecture, Canadian Geotechnical Journal, Vol.26, No.4, pp.499-516.

Burland, J.B., 1995. Closing Remarks, Proceedings, First International Symposium on Pre-Failure Deformation of Geomaterials, Sapporo, Japan, 2: 703-705.

Hill, K.O., Fujii, F., Johnson, D.C., and Kawasaki, B.S., 1978. Photosensitivity on Optical Fibre Waveguides: Application to Reflection Filter Fabrication, Applied Physics Letter, 32: 647-649.

Kersey, A.D., 1992. Multiplexed fiber optic sensors, Proceedings, Fiber Optic Sensors, Boston, Massachusetts, Eric Udd, editor, sponsored by SPIE-The International Society for Optical Engineering, pp.200-227.

Rao, Y.-J, 1998. Fiber Bragg grating sensors: principles and applications, Optic Fiber Sensor Technology, Vol.2, Edited by K.T.V. Gattan and B.T. Meggitt, Published by Chapman & Hall, London, pp.355-379.

Smith, P.D.K., and Burland, J.B., 1976. Performance of a high precision multi-point borehole extensometer in soft rock. Canadian Geotechnical Journal, 13(2): 172-176.

Takada, Y., 1965. The Internal Monitoring of Slope Movements, Disaster Prevention Research Annual Report, Disaster Prevention Research Center, Kyoto University, Kyoto, Japan, No.8, 586p (in Japanese)